Mon. Not. R. Astron. Soc. **343,** 1013–1024 (2003)

A charge-coupled device study of high-latitude Galactic structure: testing the model parameters

S. Karaali,[1,2]★ S. G. Ak,[1] S. Bilir,[1] Y. Karataş[1] and G. Gilmore[2]†

[1]*Istanbul University Science Faculty, Department of Astronomy and Space Sciences, 34452 University-Istanbul, Turkey*
[2]*Institute of Astronomy, Madingley Road, Cambridge CB3 0HA*

Accepted 2003 April 28. Received 2003 April 16; in original form 2002 November 1

ABSTRACT

We interpret published charge-coupled device (CCD) *UBVI* data to deduce the stellar density distribution and metallicity distribution function in the region of 2–8 kpc from the Galactic plane, and compare our results to several star-count models. A feature of extant star-count models is degeneracy between the adopted scaleheights of the thin and thick discs, and their local normalization. We illustrate the utility of this small data set, and future larger sets (e.g. Sloan Digital Sky Survey, SDSS), by explicitly considering consistency between the derived density laws, and the implied solar neighbourhood luminosity function. Our data set, from Hall et al.'s 1996 paper ($l = 52^\circ$, $b = -39^\circ$), contains 566 stars, selected to be consistent with stellar loci in colour–colour diagrams. The effective apparent V-magnitude interval is $15.5 \leqslant V_\mathrm{o} \leqslant 20.5$. Our analysis supports the parametrization of the recent (SDSS) galaxy model of Chen et al., except in preferring the stellar halo axial ratio to be $\eta = 0.84$.

Photometric metal abundances have been derived for 329 stars with $(B - V)_\mathrm{o} \leqslant 1.0$ using a new calibration. This shows a multimodal distribution with peaks at [Fe/H] $= -0.10$, -0.70 and -1.50 and a tail down to -2.75 dex. The vertical distance-dependent metallicity distribution function, if parametrized by a single mean value, can be described by a metallicity gradient d[Fe/H]/d$z \sim -0.2$ dex kpc^{-1} for the thin disc and thick disc, and d[Fe/H]/d$z \sim -0.1$ dex kpc^{-1} for the inner halo, to $z = 8$ kpc. However, the data are better described as the sum of three discrete distribution functions, each of which has a small or zero internal gradient. The changing mix of thin disc, thick disc and halo populations with distance from the plane generates an illusion of a smooth gradient.

Key words: methods: data analysis – stars: luminosity function, mass function – Galaxy: abundances – Galaxy: structure.

1 INTRODUCTION

The traditional star-count analyses of Galactic structure have provided a picture of the basic structural and stellar populations of the Galaxy. Examples and reviews of these analyses can be found in Bahcall (1986), Gilmore, Wyse & Kuijken (1989), Majewski (1993), Robin, Reylé & Crézé (2000) and recently Chen et al. (2001). The largest of the observational studies prior to the Sloan Digital Sky Survey (SDSS) are based on photographic surveys. The Basle Halo Program (Becker 1965) has presented the largest systematic photometric survey of the Galaxy (Del Rio & Fenkart 1987; Fenkart 1989a,b,c,d; Fenkart & Karaali 1987, 1990, 1991). The Basle Halo Program photometry is currently being recalibrated and reanalysed, using an improved calibration of the *RGU* photometric system (Buser, Rong & Karaali 1998, 1999; Ak, Karaali & Buser 1998; Karataş, Karaali & Buser 2001). More recent and future studies are being based on charge-coupled device (CCD) survey data. Most have in general much smaller area coverage or a restriction to only high Galactic latitudes, or a focus at faint magnitudes (e.g. Chen et al. 2001; Willman et al. 2002). *Hubble Space Telescope* studies are a limiting case (e.g. Johnson et al. 1999), with very deep but extremely small area coverage, and corresponding very poor statistical weight. The general absence of CCD *UV* data additionally makes such analyses sensitive to assumptions on metallicity distributions.

Even small-area CCD studies probing intermediate apparent magnitudes can be valuable, however, when analysed in the light of known solar neighbourhood constraints, especially consistency with the local stellar luminosity function. This is required since star-count analyses are essentially an attempt to deconvolve the product of a

★Visiting Astronomer, Institute of Astronomy, Cambridge.
†E-mail: gil@ast.cam.ac.uk

density profile and a local normalization, with that local normalization being the solar neighbourhood luminosity function for the specific stellar population of relevance. The local luminosity function determined from *Hipparcos* parallax data and that deduced from star-count analyses must be consistent, providing an additional constraint on Galactic modelling, or an independent check on photometric calibrations. Here we illustrate this consistency by analysing the small-area five-colour *UBVRI* CCD survey by Hall et al. (1996).

We do not here use the available SDSS data, partly since these have recently been analysed by Chen et al. (2001), but also since our aim is to illustrate the general approach. Over the next few months massive photometric data sets will become available from SDSS, 2MASS, DENIS, UKIDSS, VST, CFH/Megacam, Suprime, ... These data sets will combine statistical weight with the wide-area coverage that will allow consideration of second-order effects, quantifying the structure of the Galaxy beyond simple analytic smooth functions. Given that, it is timely now to consider method, rather than specific interim results.

In addition to a direct test of the density profile/luminosity function consistency requirements, we use the information available in the multicolour photometry, especially the U-band data, to derive limits on metallicity gradients in the thin disc, thick disc and halo.

The existence of a clear vertical metallicity gradient for any pressure-supported component of the Galaxy means that it formed by dissipative collapse. The pioneers of this suggestion are Eggen, Lynden-Bell & Sandage (1962, hereafter ELS), who argued that the Galaxy collapsed in a free-fall time ($\sim 2 \times 10^8$ yr). A discussion of the current status of this model is provided by Gilmore et al. (1989). Over the past 20 yr, observational studies have revealed that the collapse of the Galaxy occurred slowly with the limiting case being assembly of the Galaxy on many dynamical times, which (now allowing for a dark matter halo) implies times of very many Gyr (e.g. Yoshii & Saio 1979; Norris, Bessell & Pickles 1985, hereafter NBP; Norris 1986; Sandage & Fouts 1987; Carney, Latham & Laird 1990; Norris & Ryan 1991; Beers & Sommer-Larsen 1995). This picture was postulated largely on a supposed wide age in the globular cluster system (Searle & Zinn 1978, hereafter SZ; Schuster & Nissen 1989). SZ especially argued that the Galactic halo was not formed in an ordered collapse, but from merger or accretion of numerous fragments, such as dwarf-type galaxies. Such a scenario indicates no metallicity gradient or young and even more metal-rich objects at the outermost part of the Galaxy. The globular cluster age range supposition has been disproved by recent analyses (Rosenberg et al. 1999), while the number of young field halo stars has been shown to be extremely small, inconsistent with the model, by Unavane, Wyse & Gilmore (1996) and (Preston & Sneden 2000, see also Gilmore 2000). None the less, hierarchical models have become the default (Freeman & Bland-Hawthorn 2002). We readdress the metallicity gradient from the present data.

In Section 2, we describe the selection of the sample (566 stars) from the 4462 objects (stars, galaxies, quasars, etc.) observed by Hall et al. (1996), separation of the sample stars into different populations, and their absolute magnitude determination. Section 3 discusses the density functions, for seven absolute magnitude intervals evaluated for distances beyond $r = 0.4$ kpc, with three galactic models and comparison of the resulting luminosity functions with that of *Hipparcos* (Jahreiss & Wielen 1997) and Gliese & Jahreiss (1992). In Section 4, we search for a metallicity gradient in each of the galactic components, i.e. thin disc, thick disc and halo. Section 5 provides a summary and discussion. Finally, a summary is given for the new calibration in an appendix.

2 DATA

2.1 Star–galaxy–quasar separation

The data are taken from the catalogue of Hall et al. (1996), who provide a deep multicolour survey for 12 CCD fields. From the 4462 sources they detected, we selected the stellar-like sources labelled with 's', 'sf' or 'Fs' in the catalogue for Field 21e-w (Galactic coordinates $l = 52^\circ$, $b = -39^\circ$, area 0.149 deg^2). We adopted the mean of two $E(B-V)$ colour excesses given by Hall et al. (1996), i.e. 0.0223 mag, for all stars and we dereddened $U-B$ and $V-I$ colour indices by the following well-known equations:

$$E(U-B) = 0.72E(B-V) + 0.05E^2(B-V) \quad (1)$$

and

$$E(V-I) = 1.250[1 + 0.06(B-V)_\mathrm{o} + 0.014E(B-V)]E(B-V). \quad (2)$$

The total absorption $A(V)$ is evaluated as usual, i.e.

$$A(V) = 3.1E(B-V).$$

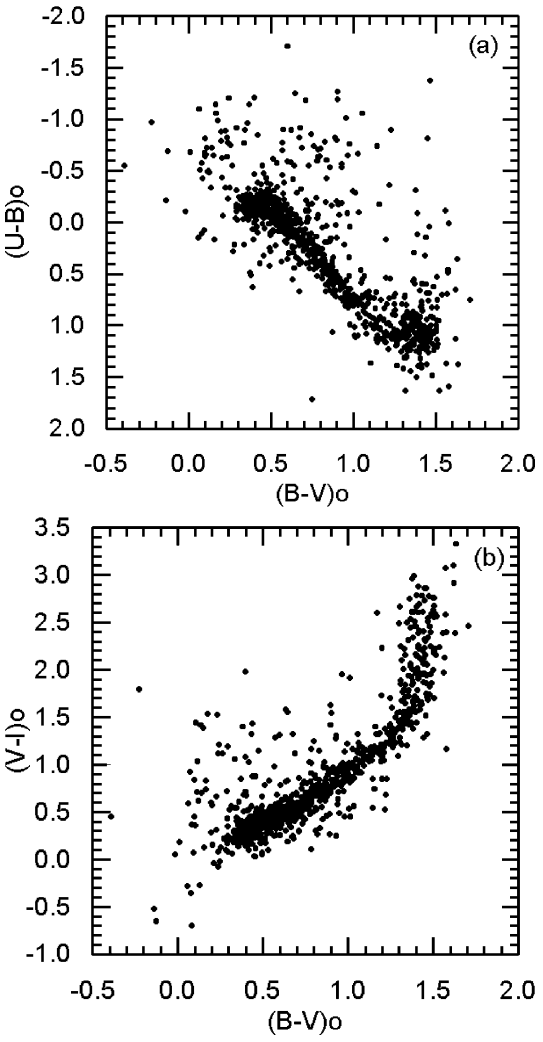

Figure 1. Two-colour diagrams for 922 objects with stellar image profiles from Hall et al. (1996): (a) for $(U-B)_\mathrm{o}$ versus $(B-V)_\mathrm{o}$, and (b) for $(V-I)_\mathrm{o}$ versus $(B-V)_\mathrm{o}$. Objects with $(U-B)_\mathrm{o} < -0.46$ mag, corresponding to $(u'-g')_\mathrm{o} < -0.5$ mag in the Sloan photometry, are extragalactic objects.

We restricted the sample at the faint end, corresponding to the peak in the distribution of apparent magnitudes, at $V_o = 20.5$ mag, leaving 922 sources. The two-colour diagrams $(U - B)_o$ versus $(B - V)_o$ and $(B - V)_o$ versus $(V - I)_o$ for these objects indicate residual significant contamination by extragalactic objects (galaxies and quasars) and WD and BHB stars (Figs 1a and b). We then rejected all sources with $(U - B)_o < -0.46$, which corresponds to the location of the bluest extragalactic objects, $(u' - g')_o < -0.5$ mag, in SDSS (Chen et al. 2001). This $(U - B)$ cut removed most outliers in the (BVI) two-colour diagrams (Fig. 2). We further removed those few sources that lay significantly off the stellar locus in $(UBVI)$, limiting the sample to 566 sources with stellar colours (Fig. 3).

2.2 Stellar population types and absolute magnitude determination

The $(B - V)_o$ colour distribution of the sample stars shows a bimodal distribution (Fig. 4), as expected for a high-latitude field (see e.g. Phleps et al. 2000). In order to assign (statistical) distances, we need to distinguish (statistically) between the three basic metallicity-dependent populations: thin disc, thick disc and halo. It is well known (cf. Chen et al. 2001 for a recent discussion) that population types are a complex function of both colour and apparent magnitude. According to Chen et al., the halo has a turnoff at $(g' - r')_o = 0.20$ mag and it dominates in the apparent magnitude interval fainter than $g'_o \sim 18$ mag, whereas the thick disc has a turnoff at $(g' - r')_o = 0.33$ mag and it is dominant at brighter apparent magnitudes, $g'_o < 18$ mag. The corresponding turnoff colours in the *UBVRI* system are $(B - V)_o = 0.41$ and 0.53 mag for halo and thick disc, respectively. The V_o versus $(B - V)_o$ diagram in Fig. 5 reveals these three populations, with, for example, the blueshift of the turnoff moving from thick disc to halo being apparent near $V = 18$. It seems that thick disc and halo populations overlap in Fig. 4. Hence, the colour distribution of the sample stars is given as a function of apparent magnitude (Fig. 6) and the turnoffs for thick disc and halo, as well as for thin disc, are fixed precisely (Table 1).

Assignments of individual absolute magnitudes for stars classified into the different populations are determined by means of appropriate colour–absolute magnitude relations, as follows. The $M(V)$ absolute magnitudes and $(B - V)_o$ of Lang (1992) are used to define the colour–absolute magnitude relation for thin disc stars (Fig. 7a). The colour–absolute magnitude relation for thick disc stars is adopted from the globular cluster 47 Tuc ([Fe/H] = −0.65 dex),

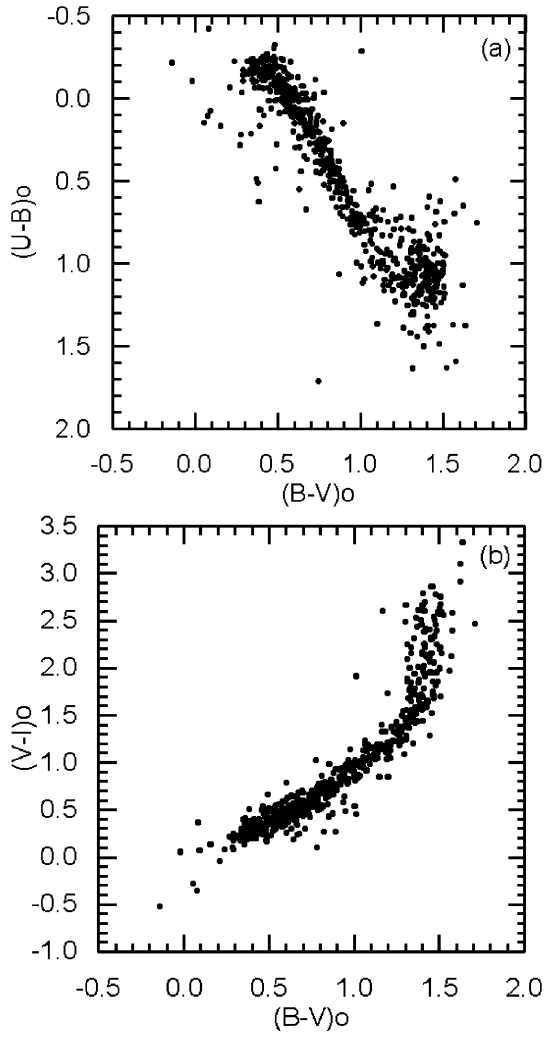

Figure 2. Two-colour diagrams for objects with $(U - B)_o \geqslant -0.46$ and $V_o \leqslant 20.5$: (a) for $(U - B)_o$ versus $(B - V)_o$, and (b) for $(V - I)_o$ versus $(B - V)_o$. The $U - B$ selection has reduced the scatter relative to that in Figs 1(a) and (b).

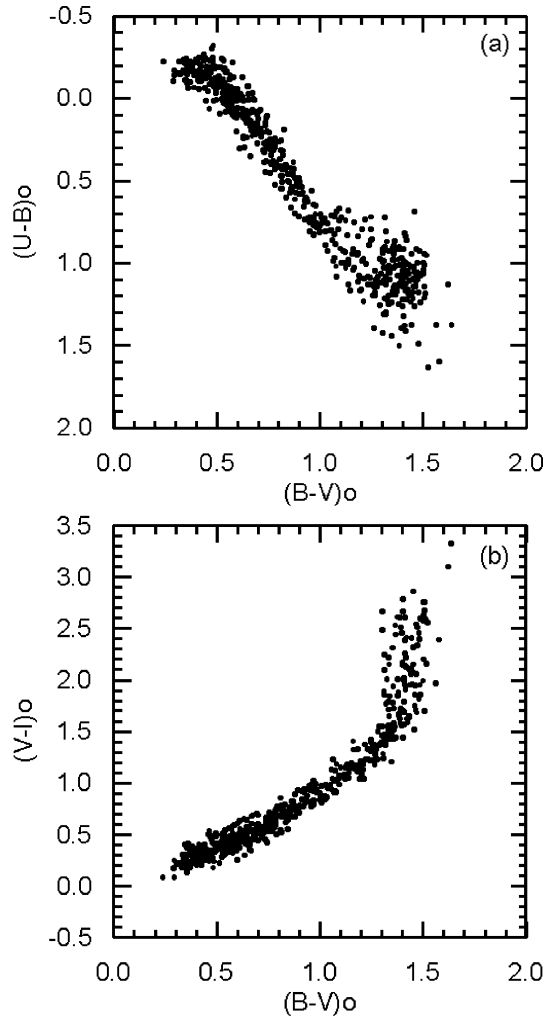

Figure 3. Two-colour diagrams for the final sample after excluding outliers in Figs 2(a) and (b): (a) for $(U - B)_o$ versus $(B - V)_o$, and (b) for $(V - I)_o$ versus $(B - V)_o$.

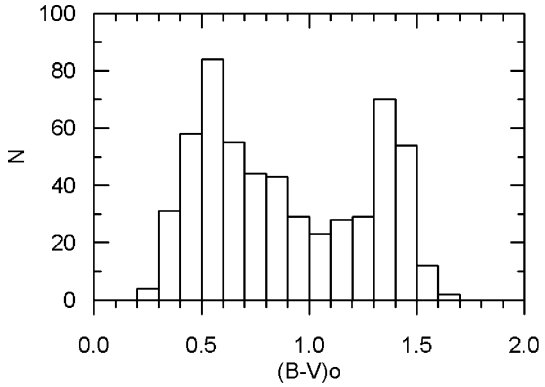

Figure 4. Colour distribution for 566 stars in our sample. The thin disc population, $(B-V)_o > 1.0$ mag, is rather conspicuous, whereas thick disc and halo populations, $(B-V)_o < 1.0$, overlap.

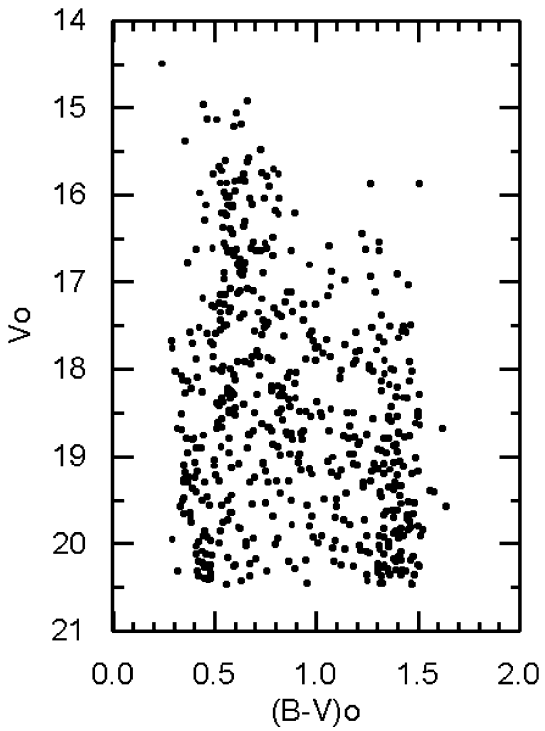

Figure 5. V_o versus $(B-V)_o$ diagram for the sample stars. Contrary to the distribution in Fig. 4, thick disc and halo stars can be distinguished, with, for example, the appearance of a blue halo turnoff being apparent near $V_o = 17.5$, $(B-V)_o = 0.4$.

with data taken from Hesser et al. (1987). These authors provide V and $B-V$ data as well as $E(B-V)$ colour excess (0.04 mag) and apparent distance modulus, $V - M(V) = 13.40$ mag, which gives the absolute magnitude of a star by combination with the total absorption, $A(V) = 3.1\ E(B-V)$ (Fig. 7b). For the halo, we used two colour–absolute magnitude relations, that for the globular cluster M13 ([Fe/H] $= -1.40$ dex) for stars with $(B-V)_o \geqslant 0.40$ mag, and that for the globular cluster M92 ([Fe/H] $= -2.20$ dex) for only an interval less than 1 mag that is not covered by the diagram of M13 ($0.30 < (B-V)_o \leqslant 0.40$). We applied the same procedure as noted above for the calibration of 47 Tuc to the data of Richer & Fahlman (1986) and Stetson & Harris (1988). Richer & Fahlman provide $E(B-V) = 0.02$ mag and $V - M(V) = 14.50$ mag for M13, while Stetson & Harris give $E(B-V) = 0.02$ mag and

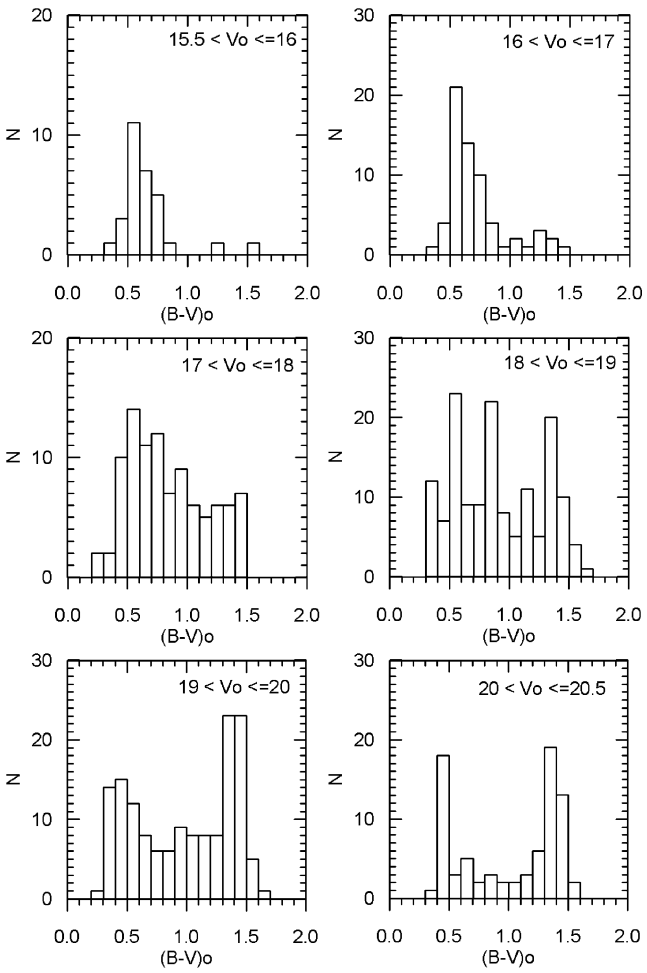

Figure 6. Colour distributions for 566 stars in our sample as a function of apparent magnitude. The colour limits revealed from these panels, which allow subpopulation isolation, are given in Table 1.

$V - M(V) = 14.60$ mag for M92. The colour–absolute magnitude relations for M13 and M92 are given in Figs 7(c) and (d).

3 DENSITY FUNCTIONS AND LUMINOSITY FUNCTION

The logarithmic space densities $D^* = \log D + 10$ are evaluated for stars for seven absolute magnitude intervals, i.e. $4 < M(V) \leqslant 5$, $5 < M(V) \leqslant 6$, $6 < M(V) \leqslant 7$, $7 < M(V) \leqslant 8$, $8 < M(V) \leqslant 9$, $9 < M(V) \leqslant 10$ and $10 < M(V) \leqslant 11$ mag, over the distance range for which absolute magnitudes are completely sampled by the available photometry (Table 2). The number of stars brighter than $M(V) = 4$

Table 1. The colour–magnitude intervals most appropriate for statistical discrimination of the three stellar populations.

Populations		$(B-V)_o$	
V_o	Thin disc	Thick disc	Halo
(15.5–16.0]	$\geqslant$0.9	<0.9	–
(16.0–17.0]	$\geqslant$0.9	<0.9	–
(17.0–18.0]	$\geqslant$0.9	<0.9	–
(18.0–19.0]	$\geqslant$1.0	[0.5–1.0)	<0.5
(19.0–20.0]	$\geqslant$0.9	–	<0.9
(20.0–20.5]	$\geqslant$0.9	–	<0.9

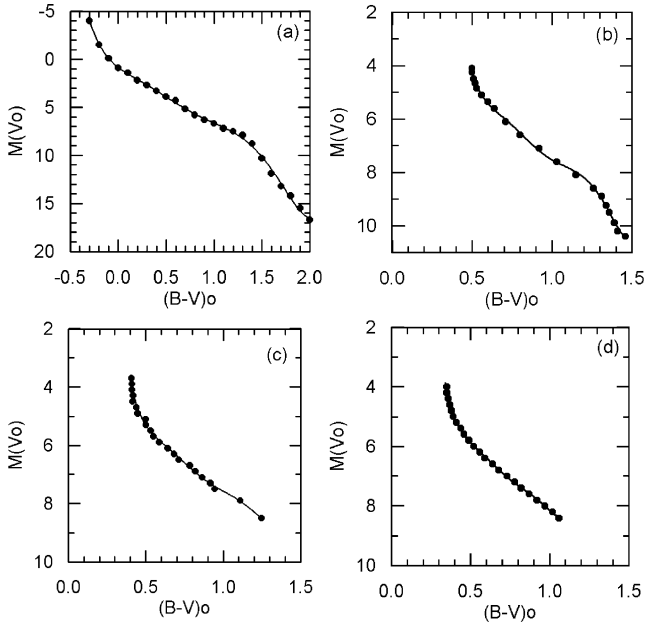

Figure 7. $M(V)$ versus $(B-V)_o$ colour–absolute magnitude relations for three populations: (a) for thin disc, (b) for thick disc, and (c) and (d) for halo (see text for details).

is also given in the same table. Here, $D = N/\Delta V_{1,2}$, N being the number of stars found in the volume $\Delta V_{1,2}$, which is determined by its limiting distances r_1 and r_2 and by the apparent field size in deg^2, $\square$, i.e.

$$\Delta V_{1,2} = \left(\frac{\pi}{180}\right)^2 \left(\frac{\square}{3}\right)\left(r_2^3 - r_1^3\right).$$

The density functions are most conveniently presented in the form of histograms whose sections with ordinates $D^*(r_1, r_2)$ cover the distance intervals (r_1, r_2). Heavy dots on the histogram sections $D^*(r_1, r_2)$ designate the centroid distance

$$r^* = \left[\left(r_1^3 + r_2^3\right)/2\right]^{1/3}$$

of the corresponding partial volume $\Delta V_{1,2}$ (Del Rio & Fenkart 1987; Fenkart & Karaali 1987; Fenkart 1989a,b,c,d). The density functions are compared with three galactic models, i.e. Gilmore & Wyse (1985, GW), Buser et al. (1998, 1999, BRK) and Chen et al. (2001, C), given in the form $\Delta \log D(r) = \log D(r, l, b) - \log D(0, l, b)$ versus r, where $\Delta \log D(r)$ is the logarithmic difference of the densities at distances r and at the Sun. Thus, $\Delta \log D(r) = 0$ is the logarithmic space density at $r = 0$, which is the parameter required for luminosity function determination. The comparison is carried out as explained in several studies of the Basle fields (Del Rio & Fenkart 1987; Fenkart & Karaali 1987), i.e. by shifting the model curve perpendicular to the distance axis until the best fit to the histogram results at the centroid distances. Fig. 8 shows the comparison of the observed density functions with the BRK model as an example.

There is adequate agreement between both models and the observed density functions within the limiting distance of completeness marked by horizontal short lines in Table 2. However, this is not the case when one includes the luminosity functions. As cited above, the luminosity function close to the Sun, $\varphi^*(M)$, i.e. the logarithmic space density for the stars with $M \pm 0.5$ mag at $r = 0$, is the D^* value corresponding to the intersection of the model curve with the ordinate axis of the histogram concerned. The luminosity functions resulting from comparisons of our space density data with the GW, BRK and C models confronted to the luminosity function of *Hipparcos* from Jahreiss & Wielen (1997, Hip 1997) and that from Gliese & Jahreiss (1992. GJ 1992) are given in Figs 9(a), (b) and (c), respectively.

When we compare the luminosity functions obtained in this work with the luminosity function from *Hipparcos*, the BRK model is most successful for intrinsically bright stars, $M(V) \leqslant 8$ mag, whereas the C model fits the data better for intrinsically fainter stars, $M(V) > 8$ mag. Obviously, the reason for the difference in this comparison of effective local luminosity functions is due to the difference between the parameters used (Table 3). For the GW and BRK models, the main difference is between the scaleheight and local density of the thick disc, whereas for BRK and C models, the differences involve five parameters, i.e. the scaleheights and scalelengths of the thin and thick discs, and the axial ratio of the halo. The effect of the different density law (power law) used for the halo in the model of Chen et al. (2001) will be discussed below.

We modified the C model by changing the halo axial ratio from their adopted 0.55 to 0.65 and 0.84, respectively. The luminosity

Table 2. Logarithmic space densities $D^* = \log D + 10$ for seven absolute magnitude intervals, where $D = N/\Delta V_{1,2}$, N being the number of stars found in the partial volume $\Delta V_{1,2}$, which is determined by its limiting distances r_1 and r_2 and by the apparent field size in deg^2, $\square$; i.e. $\Delta V_{1,2} = (\pi/180)^2(\square/3)(r_2^3 - r_1^3)$. Here $r^* = [(r_1^3 + r_2^3)/2]^{1/3}$ is the centroid distance of the partial volume $\Delta V_{1,2}$. The two short horizontal lines for each absolute magnitude interval define the distance interval for completeness (distances in kpc, volumes in pc^3).

r_1–r_2	$\Delta V_{1,2}$	$M(V) \rightarrow$ r^*	(2–3] *ND**	(3–4] *ND**	(4–5] *ND**	(5–6] *ND**	(6–7] *ND**	(7–8] *ND**	(8–9] *ND**	(9–10] *ND**	(10–11] *ND**
0.00–0.40	9.54(02)	0.32							17.02	37.50	17.02
0.40–0.63	2.85(03)	0.54						2 6.85	6 7.32	9 7.50	77.39
0.63–1.00	1.13(04)	0.86				5 6.64	13 7.06	3 6.42	17 7.18	167.15	5 6.64
1.00–1.59	4.51(04)	1.36			4 5.95	226.69	21 6.67	14 6.49	196.62	28 6.79	1 5.35
1.59–2.51	1.80(05)	2.15			135.86	27 6.18	44 6.39	266.16	25 6.14	4 5.35	
2.51–3.98	7.15(05)	3.41			13 5.26	25 5.54	275.58	19 5.42	3 4.62		
3.98–6.31	2.85(06)	5.40			17 4.78	22 4.89	18 4.80	4 4.15			
6.31–7.94	3.78(06)	7.22		2 3.72	9 4.38	74.27	4 4.02				
7.94–10.00	3.78(06)	9.09		3 3.60	12 4.20	3 3.60					
10.00–12.59	1.51(07)	11.44	1 –	2 3.12	103.82	7 3.67					
12.59–15.85	3.00(07)	14.40		3 3.00	6 3.30						
15.85–17.78	2.48(07)	16.87			3 3.08						
		Total	1	10	87	118	127	68	71	60	14

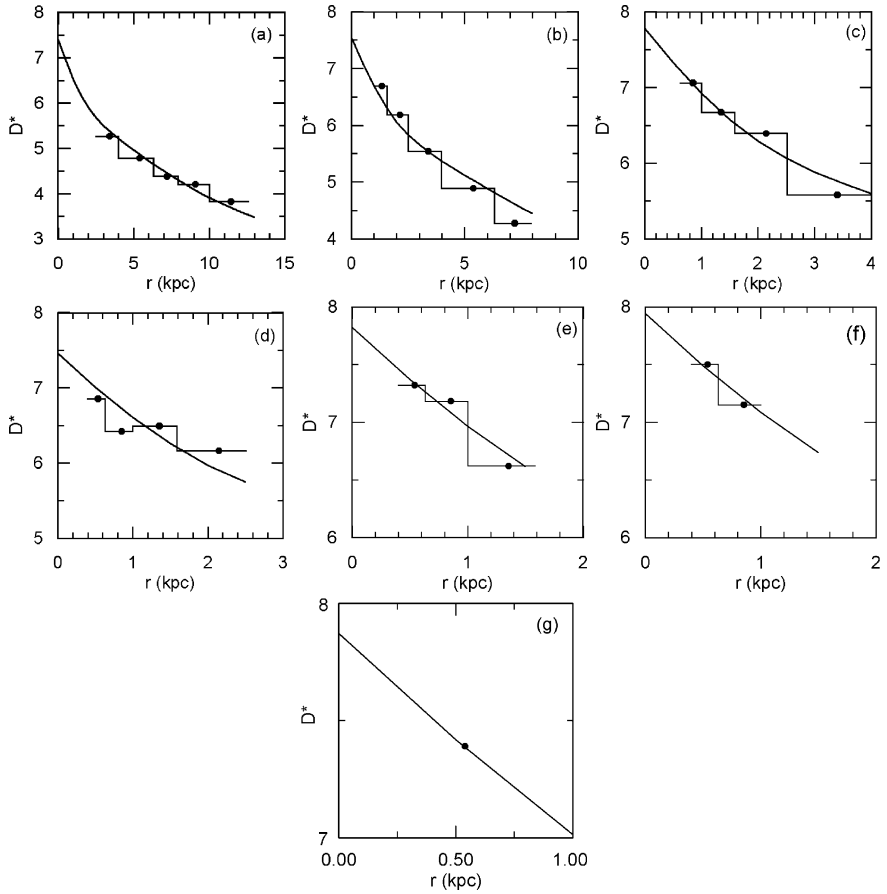

Figure 8. Comparison of logarithmic space densities with the galactic (Buser et al. 1998, 1999, BRK) model for (a) $4 < M(V) \leqslant 5$, (b) $5 < M(V) \leqslant 6$, (c) $6 < M(V) \leqslant 7$, (d) $7 < M(V) \leqslant 8$, (e) $8 < M(V) \leqslant 9$, (f) $9 < M(V) \leqslant 10$ and (g) $10 < M(V) \leqslant 11$ mag. Heavy dots designate the centroid distance $r* = [(r_1^3 + r_2^3)/2]^{1/3}$ of the corresponding partial volume $\Delta V_{1,2}$.

Table 3. Model parameters of Buser et al. (1998, 1999, BRK), Gilmore & Wyse (1985, GW) and Chen et al. (2001, C) and their comparison (fifth and sixth columns). Symbols: $n_i (i = 0, 1, 2, 3)$, local density relative to thin disc; $H_i (i = 0, 1, 2)$, scaleheight in pc; $h_i (i = 0, 1, 2)$, scalelength in pc; $R_{\rm eff}$, effective radius in pc; $R_\odot$, distance of the Sun to the Galactic Centre in pc; η, axial ratio for halo; and r_c, core radius in pc.

Authors	BRK	GW	C	BRK − GW	BRK − C
Thin disc	Double exponential	Double exponential	Double exponential	–	–
n_0	0.2[a]	0.2	0.2[a]	–	–
n_1	1.0	1.0	1.0	–	–
H_0	170	100	90	–	80
H_1	292.5	300	330	–	–
h_1	4010	4000	2250	–	1760
Thick disc	Double exponential	Double exponential	Double exponential	–	–
n_2	0.059	0.02	0.075	–	–
H_2	910	1000	750	90	160
h_2	3000	4000	3500	–	500
Halo	de Vaucouleurs	de Vaucouleurs	Power law	–	–
n_3	0.0005	0.001	0.00125	–	–
$R_{\rm eff}$	2696	2700	–	–	–
η	0.84	0.85	0.55	–	0.29
$R_\odot$	8600	8500	8600	–	–
Power-law index	–	–	2.5	–	–
r_c	–	–	1000	–	–

Note: [a]adopted.

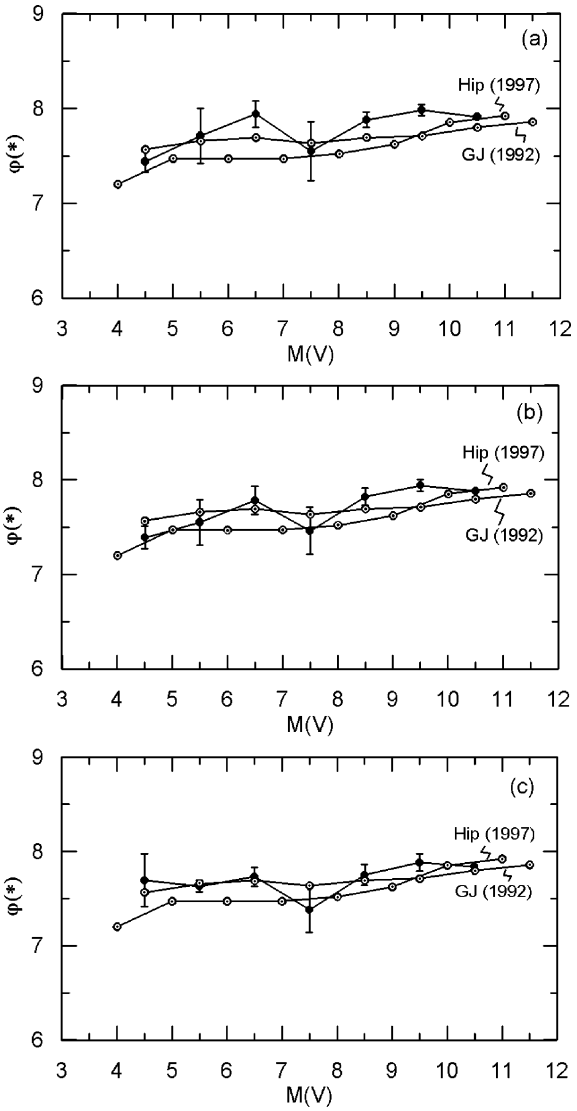

Figure 9. The stellar luminosity functions, at $r = 0$ kpc, resulting from comparisons of derived space densities with galactic models, (a) Gilmore & Wyse (1985, GW), (b) Buser et al. (1999, BRK) and (c) Chen et al. (2001, C), compared to that of *Hipparcos* (Jahreiss & Wielen 1997 = Hip 1997) and (Gliese & Jahreiss 1992 = GJ 1992).

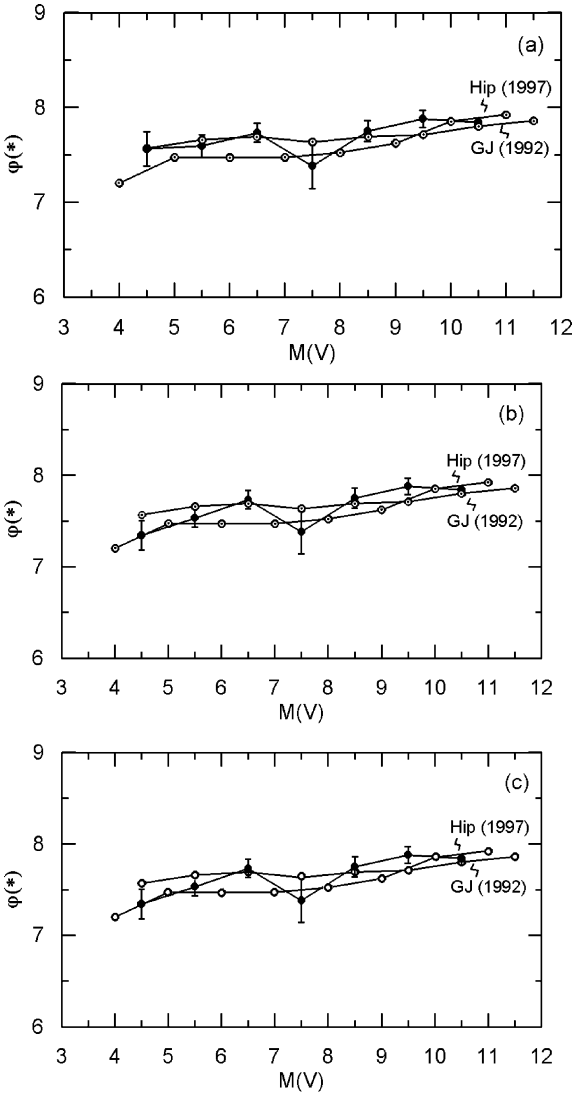

Figure 10. The stellar luminosity function, at $r = 0$ kpc, resulting from comparisons of derived space densities with the galactic model of Chen et al. (2001, C), with some modifications. In (a) and (b) the axial ratio for the halo is adopted as 0.65 and 0.84 respectively, and in (c) the density law for the halo is assumed to be de Vaucouleurs instead of power law (with axial ratio 0.84). Comparison of these luminosity functions with that of *Hipparcos* from Jahreiss & Wielen (1997, Hip 1997) and that from Gliese & Jahreiss (1992, GJ 1992) favours the models in the lower two panels.

function resulting from comparison of this modified model with the observed density functions is in substantially improved agreement with the luminosity function of *Hipparcos*. This modified model matches the data better overall than does the BRK model (Figs 10a and b). Now, a question arises from this comparison as to whether or not a power law for the halo density matches the observations to the Galactic models better. We therefore recalculated the C model, adopting a de Vaucouleurs spheroid density law (with axial ratio 0.84) for the halo in place of the Chen et al. power law. Comparison of this new model with the local normalization data (Fig. 10c) shows an improved fit, relative to the power-law model. Hence, regarding the best fit of the local luminosity function constraint resulting from comparison of the observed density functions for absolute magnitude intervals $4 < M(V) \leqslant 5$, $5 < M(V) \leqslant 6$, $6 < M(V) \leqslant 7$, $7 < M(V) \leqslant 8$, $8 < M(V) \leqslant 9$, $9 < M(V) \leqslant 10$ and $10 < M(V) \leqslant 11$, we conclude that the data suggest an increase in the axial ratio in the density law for the halo, to a value of $\eta = 0.84$, and further slightly prefer a halo density profile described by a de Vaucouleurs profile rather than a power law.

4 METALLICITY DISTRIBUTION

The metal abundances for 329 stars with $(B - V)_o \leqslant 1.0$ mag were evaluated by means of a new calibration, of the standard metallicity-dependent ultraviolet-excess photometric parameter $\delta_{0.6}$, i.e.

$$[\mathrm{Fe/H}] = 0.10 - 2.76\delta - 24.04\delta^2 + 30.00\delta^3,$$

obtained via 88 dwarfs, where the determination of abundances for most of them is based on high-resolution spectroscopy (Karaali et al. 2003). The metallicity distribution for the sample of all stars is multimodal (Table 4 and Fig. 11g); one sees three local maxima,

Table 4. Metallicity distribution for 329 stars of all apparent magnitudes (column 4) and for individual apparent magnitude intervals (columns 5–10), and the corresponding modes.

[Fe/H] (dex)	$V_o \rightarrow$ $\langle$ [Fe/H] $\rangle$ (dex)	(15.5–20.5] *N*	(15.5–16.0] *N*	(16–17] *N*	(17–18] *N*	(18–19] *N*	(19–20] *N*	(20.0–20.5] *N*
(−3.0)–(−2.8)	−2.9							
(−2.8)–(−2.6)	−2.7	1					1	
(−2.6)–(−2.4)	−2.5	2			1	1		
(−2.4)–(−2.2)	−2.3	5				3	2	
(−2.2)–(−2.0)	−2.1	9		1	1	1	4	2
(−2.0)–(−1.8)	−1.9	13				3	5	5
(−1.8)–(−1.6)	−1.7	14		1	1	5	6	1
(−1.6)–(−1.4)	−1.5	18			4	2	5	7
(−1.4)–(−1.2)	−1.3	11		1	1	5	3	1
(−1.2)–(−1.0)	−1.1	28	1	2	5	8	8	4
(−1.0)–(−0.8)	−0.9	28	3	2	3	7	10	3
(−0.8)–(−0.6)	−0.7	39	5	5	9	9	7	4
(−0.6)–(−0.4)	−0.5	21	2	4	6	5	3	1
(−0.4)–(−0.2)	−0.3	43	2	10	12	14	4	1
(−0.2)– (0.0)	−0.1	50	6	12	13	10	6	3
(0.0)–(+ 0.2)	+0.1	47	6	14	11	11	5	
	Total	329	25	52	67	84	69	32
	mode 1	−0.06	0.00	+0.03	−0.13	−0.26	−0.07	–
	mode 2	−0.83	−0.72	−0.65	−0.67	−0.73	−0.92	–
	mode 3	−1.59	–	–	−1.50	−1.72	−1.70	–

at [Fe/H] = −0.10, −0.70 and −1.50 dex, and a tail down to −2.75 dex. However, one notices a systematic shift from the metal-rich stars to the metal-poor ones, when the distribution is considered as a function of apparent magnitude (Figs 11a–f). This is particularly apparent in Fig. 12, where the mean metallicity as a function of z distance is displayed. The overall distribution shows a continuous metallicity gradient d[Fe/H]/dz = −0.20 dex kpc^{-1}, up to z = 8 kpc. It is interesting that the gradient is only marginally different for the thin disc ($z < 1.5$ kpc) and thick disc ($1.5 < z < 5$ kpc), whereas the halo shows a weak, if not zero, metallicity gradient between 5 and 8 kpc, i.e. d[Fe/H]/dz = −0.10 dex kpc^{-1}, and zero at larger distances. At face value this indicates a continuous smooth vertical abundance gradient through the thick disc. However, this presentation assumes that a single parameter, the mean, is adequate to describe a distribution function that is not Gaussian, but is multimodal. Is a single parameter a valid description of the data?

To consider this in more detail, the modes are evaluated (Table 4) for the metallicity distribution in Figs 11(a)–(g), and the metallicity distributions are given for different z intervals, z being the distance of a star to the Galactic plane in Table 5. The dips in Fig. 11(g) separating three populations are statistically significant, for Hall et al. (1996) state that the external errors in their photometry as estimated from the two independent measurements of the magnitudes of each object have been shown to be consistent with the internal errors computed according to photon statistics, except for a ∼2 per cent additional uncertainty independent of magnitude. This independent check proves that the flat-fielding process, aperture correction procedures and photometry methods are all quite reliable, having inherent limitations of only the aforementioned ∼2 per cent. As for systematic errors, their stellar locus matches values for stellar colours from the literature to about 5 per cent. Three modes at [Fe/H] = −0.06, −0.83 and −1.59 dex for the distribution in Fig. 11(g) correspond to the mean metal abundance for three components of the Galaxy, i.e. thin disc, thick disc and halo, though the one for the thick disc is a bit lower than the canonical one, [Fe/H] = −0.65 dex, probably affected by the metal-poor tail of the thick disc (Norris 1996, see section 5 for detail). The Gaussian fits with the modes just cited and their sum are also shown in Fig. 11(g).

As Figs 11(a)–(f) make clear, the apparent abundance gradient is evidently an artefact of the changing relative proportions of the three populations present, thin disc, thick disc and halo, with each population having no significant gradient. Each abundance distribution is simply consistent with a sum of three discrete distributions, with no systematic change in the mode of each. This suggestion can be confirmed by the modes for individual apparent magnitude intervals (Table 4), which show fluctuations, with the exception of the mode for the thick disc for the apparent magnitude interval $19 < V_o \leqslant 20$, which is ∼ −0.2 dex lower than the ones for brighter apparent magnitude intervals. This determination, with independent high-quality data and a new much-improved photometric calibration, is essentially in agreement with the conclusions of Gilmore & Wyse (1985): the Galactic discs are better described as the sum of independent well-mixed subpopulations with different spatial distributions than as a continuum. However, the mean metal abundance in Table 5 show a systematic decrease with increasing mean z, indicating a slight vertical metallicity gradient for thin disc, thick disc and inner halo (see Section 5 for detail).

5 SUMMARY AND DISCUSSION

In this work we illustrated the capabilities of present and forthcoming analyses of CCD star-count data, when such analyses are based purely on star-by-star inversion of colour data, through stellar photometric parallax. We showed how such analyses can be robust, provided that they utilize as a constraint consistency with the local solar neighbourhood stellar luminosity function. We showed how such analyses can limit possible metallicity gradients for the components of the Galaxy, and provide the choice of best model

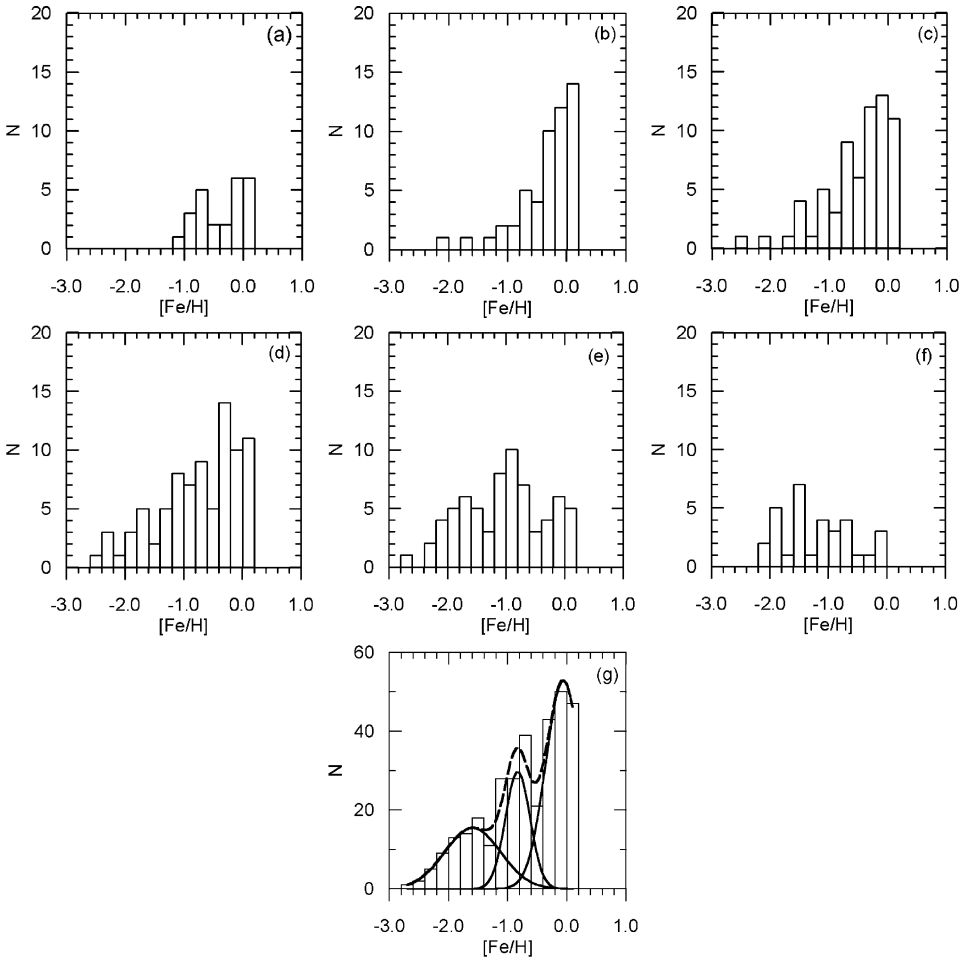

Figure 11. Metallicity distribution for stars with $(B-V)_o \leqslant 1.0$ mag as a function of apparent magnitude V_o (panels a–f), and for their combination within the limiting apparent magnitude, $V_o \leqslant 20.5$ (last panel): (a) $15.5 < V_o \leqslant 16$, (b) $16 < V_o \leqslant 17$, (c) $17 < V_o \leqslant 18$, (d) $18 < V_o \leqslant 19$, (e) $19 < V_o \leqslant 20$, (f) $20 < V_o \leqslant 20.5$ and (g) $15.5 < V_o \leqslant 20.5$. Curves in (g) are the fitted Gaussian distributions for three populations (continuous curve) and their sum (dashed curve).

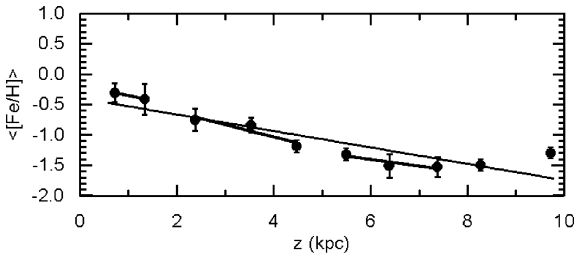

Figure 12. Mean metal abundance versus mean z distance for 10 z intervals, suggesting a metallicity gradient $d[Fe/H]/dz \sim -0.2$ dex kpc^{-1} for the thin disc and thick disc, and $d[Fe/H]/dz \sim -0.1$ dex kpc^{-1} for the inner halo. As shown in the text, this apparent smooth abundance gradient is an artefact of a mix of three independent distributions.

parameters. We now review our results and discuss them in the context of those by other authors.

(i) The use of colour data to identify and reject extragalactic objects

A considerable fraction of the star candidates of Hall et al. (1996), selected from image structure, and labelled with 's', 'sf' and 'Fs' in their work, turned out to be extragalactic objects, according to their position in the $(U-B)_o$ versus $(B-V)_o$ colour–colour diagram. An effective colour cut, consistent with those adopted by SDSS (Chen et al. 2001), is to reject all point sources with $(U-B)_o$ colour indices less than -0.46, which corresponds to $(u'-g')_o < -0.50$. Comparison of Figs 1 and 2 shows that this single selection substantially reduces scatter away from the stellar locus. Removal of objects with $(U-B)_o < -0.46$ and imposing an apparent magnitude cut at the completeness limit $V_o \leqslant 20.5$ allowed the stellar locus to be readily identified, and outliers to be excluded.

(ii) Stellar luminosity function at $r = 0$ kpc obtained from deep CCD photometry

The sample of Hall et al. (1996) does not allow space density determination for nearby stars as a result of the lack of apparently bright stars in this sample. Hence, space densities are complete at distances larger than 2.51, 1.00 and 0.63 kpc for absolute magnitude intervals $4 < M(V) \leqslant 5$, $5 < M(V) \leqslant 6$ and $6 < M(V) \leqslant 7$, respectively, and 0.40 kpc for four absolutely fainter intervals, i.e. $7 < M(V) \leqslant 8$, $8 < M(V) \leqslant 9$, $9 < M(V) \leqslant 10$ and $10 < M(V) \leqslant 11$.

In order to allow comparison with the local luminosity functions of *Hipparcos* (Jahreiss & Wielen 1997) and with that evaluated by

Table 5. Metallicity distribution for 329 stars for 10 z distance intervals, z being the distance to the Galactic plane in kpc. Mean metal abundances and mean z distances, as well as mean errors for the metallicity, are also indicated.

[Fe/H] (dex)	z (kpc) → ⟨ [Fe/H] ⟩ (dex)	(0–1] *N*	(1–2] *N*	(2–3] *N*	(3–4] *N*	(4–5] *N*	(5–6] *N*	(6–7] *N*	(7–8] *N*	(8–9] *N*	(9–10] *N*
(−3.0)–(−2.8)	−2.9										
(−2.8)–(−2.6)	−2.7					1					
(−2.6)–(−2.4)	−2.5						1				
(−2.4)–(−2.2)	−2.3			2		1			2		
(−2.2)–(−2.0)	−2.1			1	2	1	1	2		1	1
(−2.0)–(−1.8)	−1.9		1	2	1	1	1	3	3		1
(−1.8)–(−1.6)	−1.7		2	2	1	3		3	1	1	
(−1.6)–(−1.4)	−1.5	1	3	5	3	2		1	2		
(−1.4)–(−1.2)	−1.3		3	1	2	2		1	1	1	
(−1.2)–(−1.0)	−1.1	5	5	5	3	2	3	2	1		
(−1.0)–(−0.8)	−0.9	2	8	5	4	2	1	3	2	1	
(−0.8)–(−0.6)	−0.7	5	15	10	2	2	1		1		1
(−0.6)–(−0.4)	−0.5	4	5	8	3		1				
(−0.4)–(−0.2)	−0.3	10	17	7	4	3					
(−0.2)– (0.0)	−0.1	13	23	8	4	2					
(0.0)–(+ 0.2)	+0.1	15	25	5	2						
	Total	55	107	61	31	22	9	15	13	4	3
	⟨ z ⟩ (kpc)	0.75	1.37	2.41	3.57	4.50	5.53	6.42	7.42	8.30	9.75
	⟨ [Fe/H] ⟩ (dex)	−0.31	−0.41	−0.76	−0.84	−1.19	−1.32	−1.51	−1.53	1.50	−1.30
	m.e.	±0.16	±0.25	±0.18	±0.12	±0.10	±0.10	±0.19	±0.16	±0.09	±0.08

Kul (1994) from the data of Gliese & Jahreiss (1992), the star-count models themselves must be used to extrapolate the star counts to the solar neighbourhood. While in general all three models analysed are in tolerable agreement with the required local normalizations, there are differences. The model of Buser et al. (1998, 1999) fits best for three absolute magnitude intervals, i.e. $6 < M(V) \leqslant 7$, $8 < M(V) \leqslant 9$ and $9 < M(V) \leqslant 10$, relative to that of Gilmore & Wyse (1985) (Fig. 9a). This difference is due to the differences between scaleheights and local densities adopted for the thick disc (cf. Table 3). The model of Chen et al. (2001) matches the constraint well for low-luminosity local thin disc stars, for absolutely faint magnitude intervals ($M(V) > 8$), whereas the model of Buser et al. matches better for the more luminous thick disc stars, for the bright ones ($M(V) < 7$). This distinction is due to differences between five model parameters (Table 3). Additionally, one must take into account the difference density laws used for the halo for these models, i.e. de Vaucouleurs spheroid for Buser et al., and power law for Chen et al.

We determined the sensitivity of the local luminosity function constraint on determination of the axial ratio of the halo by calculating models following Chen et al. (2001) except with axial ratio $\eta = 0.65$ (Fig. 10a) and $\eta = 0.84$ (Fig. 10b). The first value (0.65) is that derived by Yanny et al. (2000) based on BHB tracers from SDSS data, and rather close to the value (0.6) suggested by Wyse & Gilmore (1988). The second value is not only equal to or close to the values proposed by Buser et al. (1998, 1999) and Gilmore & Wyse (1985), but also coincides with those cited by other authors. For example Hawkins (1984) and Bahcall & Soneira (1984) found $\eta = 0.9$ and 0.8, respectively. Preston, Shectman & Beers (1991) state that η increases from 0.5 to 1 up to 20 kpc, while Robin et al. (2000) deduced that the halo has a flattening of $\eta = 0.76$. It is interesting that the luminosity function comparison in Figs 10(a) and (b) distinguishes these models, thus showing that the flattening parameter η of the halo is the most sensitive parameter that can be distinguished here between the Buser et al. and the Chen et al. models. Finally, a de Vaucouleurs spheroid with the model parameters of Chen et al., except that $\eta = 0.84$, works well (Fig. 10c), indicating that η but not the density law for the halo plays an important role in the luminosity function comparison. Overall, we conclude that the model of Chen et al. (2001) is consistent with these data, under the condition that $\eta = 0.84$.

(iii) Vertical metallicity gradient for the three components of the Galaxy

Our data are consistent with, but do not require, weak vertical metallicity gradients in both the thin disc and thick disc. In the halo, any vertical metallicity gradient is even weaker. A better description of our data is that the metallicity distribution function is the sum of three discrete distributions, none of which has a significant metallicity gradient. Rather, an apparent vertical metallicity gradient arises from the changing contributions of the three distributions with distance from the Galactic plane. Some gradient inside each population is however allowed by our analysis.

The maximum possible vertical metallicity gradient for the thin disc, i.e. $\mathrm{d[Fe/H]}/\mathrm{d}z \sim -0.2$ dex kpc^{-1}, is consistent with many other determinations, and consistent with a convolution of a weak age–metallicity relation and age–velocity dispersion relation.

If there were a detected vertical metallicity gradient for the thick disc, this would impact some formation histories postulated for the formation of the classical thick disc. Until recently, this component of our Galaxy was assumed to have a mean metal abundance [Fe/H] ~ -0.60 dex, with a narrow metallicity range, to have a scaleheight 1.0–1.3 kpc, and to comprise some 0.02–0.05 of the material in the solar neighbourhood. Additionally, and more importantly, it was argued that the stars of the thick disc were formed from a merger into the Galaxy (cf. Norris 1996, and references within), a formation mechanism unlikely to leave an abundance gradient. Some recent analyses suggested that the thick disc is a more massive component of the Galaxy (Majewski 1993), with a metal-poor (Norris 1996) and

a metal-rich (Carney 2000; Karaali et al. 2000) tail. Hence, a revision of the formation scenario of the thick disc may be required. The work of Reid & Majewski (1993), in which a vertical metallicity gradient $d[Fe/H]/dz \sim -0.10$ dex kpc^{-1} is claimed, is consistent with our results (Fig. 12) but also consistent with a simple no-gradient mixed-population model. Chiba & Yoshii (1998) also suggest a vertical metallicity gradient for the thick disc. A substantially larger sample of stars with both metallicities and appropriate kinematics will be required to distinguish between these models (cf. Gilmore, Wyse & Norris 2002).

Detection of a metallicity gradient in the halo which changes with Galactocentric distance would be a test of scenarios suggesting important late accretion of the outermost part of the Galaxy. One might expect a gradient in the inner partly dissipatively formed halo, and none farther out, provided that the stellar velocity ellipsoid is as observed, only slightly radially anisotropic. This gradient is consistent with our results, i.e. there is a slight vertical metallicity gradient, $d[Fe/H]/dz \sim -0.10$ dex kpc^{-1}, in the inner part of the halo ($5 < z \leqslant 8$ kpc) and zero in its outer part ($8 < z \leqslant 10$ kpc). However, we recognize that there are significant statistical uncertainties, and a proper interpretation will need to await large-scale stellar surveys from the SDSS.

ACKNOWLEDGMENTS

This work was supported by the Research Fund of the University of Istanbul, Project Number 1417/050500. We thank P. B. Hall et al. (1996) for providing their data.

REFERENCES

Ak S. G., Karaali S., Buser R., 1998, A&AS, 131, 345
Bahcall J. N., 1986, ARA&A, 24, 577
Bahcall J. N., Soneira R. M., 1984, ApJS, 55, 67
Becker W., 1965, Z. Astrophys., 62, 54
Beers T. C., Sommer-Larsen J., 1995, ApJS, 96, 175
Buser R., Rong J., Karaali S., 1998, A&A, 331, 934 (BRK)
Buser R., Rong J., Karaali S., 1999, A&A, 348, 98 (BRK)
Carney B. W., 1979, ApJ, 233, 211
Carney B. W., 2000, in Noels A., Magain P., Caro D., Jehin E., Parmnetier G., Thoul A. A., eds, Proc. 35th Liége Int. Astrophys. Colloq., The Galctic Halo: From Globular Clusters to Field Stars. Inst. Astrophys. Geophys., Liege, p. 287
Carney B. W., Latham D. W., Laird J. B., 1990, AJ, 99, 572
Cayrel de Strobel G., Soubiran C., Friel E. D., Ralite N., Francois P., 1997, A&AS, 124, 299
Cayrel de Strobel G., Soubiran C., Ralite N., 2001, A&A, 373, 159
Chen B. et al., 2001, ApJ, 553, 184 (C)
Chiba M., Yoshii Y., 1998, AJ, 115, 168
Del Rio G., Fenkart R. P., 1987, A&AS, 68, 397
Eggen O. J., Lynden-Bell D., Sandage A. R., 1962, ApJ, 136, 748 (ELS)
Fenkart R. P., 1989a, A&AS, 78, 217
Fenkart R. P., 1989b, A&AS, 79, 51
Fenkart R. P., 1989c, A&AS, 80, 89
Fenkart R. P., 1989d, A&AS, 81, 187
Fenkart R. P., Karaali S., 1987, A&AS, 69, 33
Fenkart R. P., Karaali S., 1990, A&AS, 83, 481
Fenkart R. P., Karaali S., 1991, A&AS, 88, 233
Freeman K., Bland-Hawthorn J., 2002, ARA&A, 40, 487
Gilmore G., 2000, J. Br. Astron. Assoc., 110, 42
Gilmore G., Wyse R. F. G., 1985, AJ, 90, 2015 (GW)
Gilmore G., Wyse R. F. G., Kuijken K., 1989, ARA&A, 27, 555
Gilmore G., Wyse R. F. G., Norris J. E., 2002, ApJ, 574, 39
Gliese W., Jahreiss H., 1992, Third Catalogue of Nearby Stars (Preliminary Version). Astron. Rechen Inst. Heidelberg
Hall P. B., Osmer P. S., Green R. F., Porter A. C., Warren S. J., 1996, ApJS, 104, 185
Hawkins M. R. S., 1984, MNRAS, 206, 433
Hesser J. E., Harris W. E., Vandenberg D. A., Allwright J. W. B., Shott P., Stetson P. B., 1987, PASP, 99, 739
Jahreiss H., Wielen R., 1997, in Battrick B., Perryman M. A. C., Bernacca P. L., eds, Hipparcos'97 – Presentation of the Hipparcos and Tycho Catalogues and First Astrophysical Results of the Hipparcos Space Astrometry Mission, ESA SP-402. ESA Publications Division, Noordwijk, p. 675
Johnson R. A., Gilmore G., Tanvir N. R., Elson R. A. W., 1999, New Astron., 4, 431
Karaali S., Karataş Y., Bilir S., Ak S. G., Gilmore G. F., 2000, in Noels A., Magain P., Caro D., Jehin E., Parmnetier G., Thoul A. A., eds, Proc. 35th Liége Int. Astrophys. Colloq., The Galctic Halo: From Globular Clusters to Field Stars. Inst. Astrophys. Geophys., Liege, p. 353
Karaali S., Bilir S., Karataş Y., Ak S. G., 2003, Publ. Ast. Soc. Aust., 20, 165
Karataş Y., Karaali S., Buser R., 2001, A&A, 373, 895
Kul F., 1994, Master's thesis, Univ. Istanbul, Institute of Advanced Studies
Lang K. R., 1992, Astrophysical Data I – Planets and Stars. Springer, Berlin
Majewski S. R., 1993, ARA&A, 31, 575
Mermilliod J. C., Mermilliod M., Hauck B., 1997, A&AS, 124, 349
Norris J. E., 1986, ApJS, 61, 667
Norris J. E., 1996, in Morrison H. L., Sarajedini A., eds, ASP Conf. Ser. Vol. 92, Formation of the Galactic Halo....Inside and Out. Astron. Soc. Pac., San Francisco, p. 14
Norris J. E., Ryan S. G., 1991, ApJ, 380, 403
Norris J. E., Bessell M. S., Pickles A. J., 1985, ApJS, 58, 463 (NBP)
Phleps S., Meisenheimer K., Fuchs B., Wolf C., 2000, A&A, 356, 108
Preston G. W., Sneden C., 2000, AJ, 120, 1014
Preston G. W., Shectman S. A., Beers T. C., 1991, ApJS, 76, 1001
Reid N., Majewski S. R., 1993, ApJ, 409, 635
Richer H. B., Fahlman G. G., 1986, ApJ, 304, 273
Robin A. C., Reylé C., Crézé M., 2000, A&A, 359, 103
Rosenberg A., Saviane I., Piotto G., Aparicio A., 1999, AJ, 118, 2306
Sandage A., Fouts G., 1987, AJ, 93, 74
Schuster W. J., Nissen P. E., 1989, A&A, 222, 69
Searle L., Zinn R., 1978, ApJ, 225, 357 (SZ)
Stetson P. B., Harris W. E., 1988, AJ, 96, 909
Unavane M., Wyse R. F. G., Gilmore G., 1996, MNRAS, 278, 727
Willman B., Dalcanton J., Ivezic Z., Jackson T., Lupton R., Brinkmann J., Hennessy G., Hindsley R., 2002, AJ, 123, 848
Wyse R. F. G., Gilmore G., 1988, AJ, 95, 1404
Yanny B. et al., 2000, ApJ, 540, 825
Yoshii Y., Saio H., 1979, PASJ, 31, 339

APPENDIX A: THE NEW METALLICITY CALIBRATION

Data for 88 dwarfs with metallicities $-2.7 \leqslant [Fe/H] \leqslant +0.26$ dex were taken from three sources for a new metallicity calibration: (1) Some 57 of them with $\log g \geqslant 4.5$ are from Cayrel de Strobel, Soubiran & Ralite (2001), a catalogue that supplies detailed information for stars with abundance determinations based on high-resolution spectroscopy. (2) Eleven high- or intermediate-mass stars were taken from a different catalogue of the same authors (Cayrel de Strobel et al. 1997). This catalogue has the advantage of including metal-poor stars down to $[Fe/H] = -2.70$ dex with smaller gravity, i.e. $\log g \geqslant 4.0$, however. For the *UBV* magnitudes and colours, specialized catalogues that are included in the General Catalogue of Photometric Data (Mermilliod, Mermilliod & Hauck 1997) were consulted. The parallax and the galactic latitude of stars that were used in the choice of the sample stars were provided from the data base. (3) Finally, 20 stars classified as dwarfs by Carney (1979),

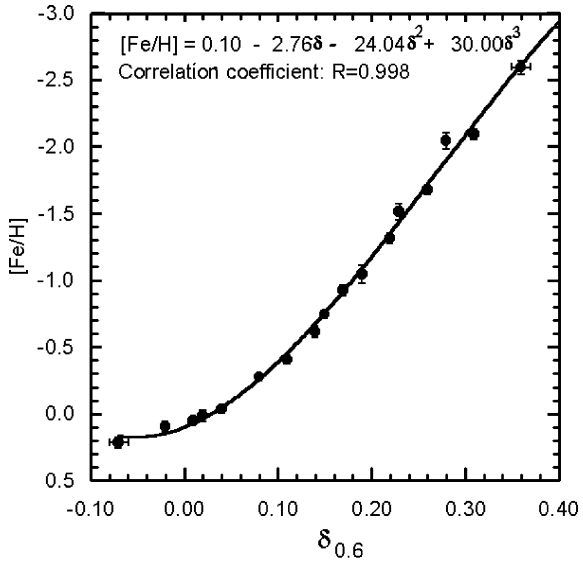

Figure A1. The third-degree polynomial curve through 17 locus points and the correlation coefficient. The bars show the mean errors.

Table A1. Locus points and the number of stars associated with them (last column). The other columns give the current number, $\delta_{0.6}$, [Fe/H], mean errors for the $\delta_{0.6}$ and [Fe/H], respectively.

No.	$\delta_{0.6}$	[Fe/H]	$\Delta\delta_{0.6}$	Δ [Fe/H]	N
1	−0.07	+0.21	0.01	0.04	3
2	−0.02	+0.09	0.00	0.04	8
3	+0.01	+0.05	0.00	0.02	7
4	+0.02	+0.01	0.00	0.04	7
5	+0.04	−0.04	0.00	0.03	7
6	+0.08	−0.28	0.00	0.03	8
7	+0.11	−0.41	0.00	0.03	7
8	+0.14	−0.62	0.00	0.04	8
9	+0.15	−0.75	0.00	0.03	5
10	+0.17	−0.93	0.00	0.04	4
11	+0.19	−1.05	0.00	0.07	3
12	+0.22	−1.32	0.00	0.04	5
13	+0.23	−1.52	0.00	0.06	3
14	+0.26	−1.68	0.00	0.03	3
15	+0.28	−2.05	0.00	0.06	4
16	+0.31	−2.10	0.00	0.04	3
17	+0.36	−2.60	0.01	0.05	3

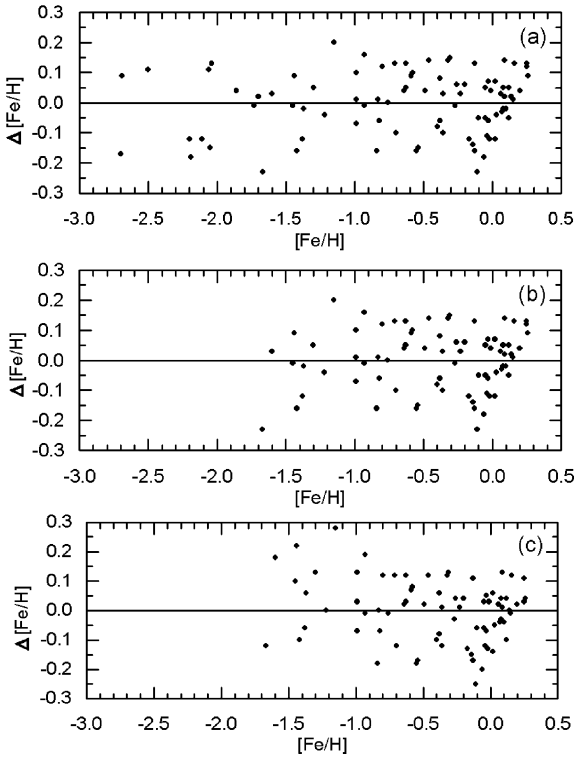

Figure A2. Deviation of evaluated metallicities from original ones versus original metallicity for (a) all stars in our sample, (b) stars with [Fe/H] $\geqslant -1.75$ dex in our sample, and (c) the sample of Carney (1979), where [Fe/H] $= -1.75$ dex is the validity limit for Carney's calibration.

who used them in his metallicity calibration, were included also in the new sample.

The full interval for normalized ultraviolet excess, $-0.09 \leqslant \delta_{0.6} \leqslant +0.38$ mag was divided into 17 sub-intervals. The centroid of each was adopted as a locus point to fit the couple ($\delta_{0.6}$, [Fe/H]). Table A1 gives the locus points and the number of stars associated, and Fig. A1 the fit of these points by a third-degree polynomial, i.e.

$$[\mathrm{Fe/H}] = 0.10 - 2.76\delta - 24.04\delta^2 + 30.00\delta^3.$$

Analysis of the deviations of metallicities deduced from this calibration compared to the original metallicity shows that the accuracy is at the level of Carney's work (Figs A2a–c).

This paper has been typeset from a TEX/LATEX file prepared by the author.